




Highly dispersed polyaniline/graphene oxide composites for corrosion protection of polyvinyl chloride/epoxy powder coatings on steel

YuYing Han¹, ZiLiang Liu¹, Shuang Wang¹, Wenxue Wang¹, ChuanXing Wang^{1,2}, and ChuanHui Gao^{1,*} 

¹College of Chemical Engineering, Qingdao University of Science and Technology, Qingdao 266024, China

²Shandong Key Laboratory of Corrosion Science, Institute of Oceanology, Chinese Academy of Sciences, Qingdao 266071, China

Received: 19 November 2020

Accepted: 9 February 2021

Published online:
26 April 2021

© The Author(s), under exclusive licence to Springer Science+Business Media, LLC, part of Springer Nature 2021

ABSTRACT

In this study, a novel functionalized graphene oxide(GO) sheet of polyaniline(PANI) was prepared by in situ polymerization of aniline. Fourier transform infrared spectroscopy (FTIR), X-ray diffractometer (XRD) and scanning electron microscope (SEM) indicated the successful polymerization of aniline on GO tablets, and PANI was uniformly inserted into the GO lamellas that benefited the dispersion of PAGO. The anticorrosion properties of PAGO-PVC/EP coatings with different contents were analyzed and compared with PAGO-0 and the GO coatings. Electrochemical analysis showed that an appropriate amount of PAGO (0.5wt%) could significantly improve the long-term corrosion resistance of the coating. Its excellent corrosion resistance was attributed to two parts: (1) PAGO had good dispersion and could improve the barrier property of the coating to block H₂O, O₂ and electrolytes from penetrating to the steel substrate; (2) PANI with complete electrical activity could timely transfer the electrons lost from the base to the coating surface, and form a passivation film composed of Fe₃O₄ and Fe₂O₃ by induction. The barrier property of GO and the self-healing ability of PANI made PAGO-based PVC/EP coatings excellent in corrosion resistance.

Introduction

For anticorrosive coating, the following conditions must be met to give full play to its excellent corrosion resistance: Firstly, the coating should have a good

barrier and have the ability to fully prevent the invasion of corrosion media. Secondly, the coating should have excellent bonding strength with the substrate, to avoid the intrusion of corrosive media, accumulation and diffusion, resulting in coating off.

Handling Editor: Jaime Grunlan.

Address correspondence to E-mail: gaochuanhui@qust.edu.cn

Thirdly, the coating should have good self-repair, be able to achieve self-repair in the state of local damage, timely prevent diffusion of corrosion media, and avoid serious corrosion to the substrate [1–4].

The barrier property of the coating mainly depends on the compactness of the coating structure. The traditional polymer resin coating is porous, which is conducive to the invasion of corrosive media [5–7]. The addition of nano filler can reduce the porosity of the coating and effectively extend the invasion path of H₂O, O₂ and other corrosive media. In recent years, GO nanocomposites have attracted great attention in corrosion protection. As an important kind of nano derivatives of graphene materials, GO also shows its excellent physical, chemical, optical and electrical properties. The introduction of oxygen-containing groups not only makes GO have chemical stability, but also provides surface modification active sites and large specific surface area for the synthesis of GO composites. As a precursor and support carrier of synthetic graphene-based composites, GO is easily functionalized and highly controllable. In the process of composite with metal, metal oxide, polymer and other materials, it can provide a large specific surface area to effectively disperse adhesion materials and prevent agglomeration [8–11].

For example, Suarva et al. [12] functionalized 4-fluorophenol/graphene oxide (FGO) by esterification and used it as a nano-filler in epoxy resin. The results showed that when 0.25wt% FGO was added to epoxy, the corrosion resistance of the coating was significantly higher than that of pure epoxy coating. Tian et al. [13] reported the study of environment-friendly waterborne epoxy coating (WBE) with GO grafted ammonium salt (AGO) as co-dispersant. The results showed that AGO sheet successfully suppressed the formation of micropores and microdefects, and a denser WBE/AGO composite coating was obtained. The results of potentiodynamic polarization test showed that the corrosion resistance of the coating had been greatly improved. The corrosion rate of the WBE/AGO coating decreased by three orders of magnitude compared to the pure WBE coating. Obviously, the dispersion of modified GO/graphene anticorrosive fillers in the coating had been significantly improved, which could give full play to the properties of graphene-based nano-fillers and improve the anticorrosive performance of the coating.

An effective anticorrosive coating should have both passive barrier and active self-healing characteristics. When the coating cracks, it can quickly induce the formation of a protective film to achieve long-term protection of the coating [14–16]. As a conductive filler, the conjugated chemical structure of polyaniline (PANI) makes it have catalytic oxidation–reduction behavior, increases the corrosion potential of metal surface, and forms a protective passivation layer on the metal surface, which can be used in anticorrosive coatings to enhance the protection of metal [17]. PANI has the advantages of high stability, easy synthesis, good acid–base chemical reversibility and low production cost. It has been widely used in the fields of battery, catalysis, anticorrosive coating, light-emitting diode and sensor [18, 19]. Meroufel et al. [20] have reported the addition of PANI into a zinc-rich primer to enhance the electronic conduction paths between zinc particles inside the coating and the steel substrate. Qiu et al. [21] prepared a composite coating of PANI-GO on 316 stainless steel by a pulse current codeposition method. Agglomeration of aniline and GO occurred during the deposition process and formed a compact coating. The corrosion inhibition efficiency and protection efficiency of the PANI-GO composite coating reached 98.4% and 99.3%, respectively.

At present, graphene/GO composite fillers are mostly used in waterborne anticorrosive coatings. However, governments all over the world attach great importance to the environmental pollution of paint factories and enterprises, and strengthen the restrictions on the use of solvents. In this context, powder coating have developed rapidly due to their pollution-free and high utilization rate of raw materials [22]. Therefore, the application of functional fossil graphene/GO composite fillers in powder coatings not only reduces the harm of solvent-based coatings to the environment, but also greatly improves the anticorrosive performance of the coatings, which provides a new technical way for the development of a new generation of functional protective coatings.

In this work, we combined the advantages of PANI and GO to improve the performance of the coatings with a small amount of PAGO that would enhance the barrier performance and self-healing ability of the PVC/EP powder coatings. Thus, a new type of PANI functionalized GO sheet (PAGO) was prepared by in situ polymerization of aniline. PANI was

uniformly inserted into the GO lamellas that benefited the dispersion of PAGO in the PVC/EP coating. To the best of our knowledge, this report is the first dealing with the corrosion performance of PVC/EP powder coatings modified by PAGO composite. The functionalized GO was characterized by Fourier transform infrared spectroscopy (FT-IR), X-ray diffraction (XRD) and scanning electron microscope (SEM). The corrosion resistance mechanism of PAGO coating was studied by electrochemical impedance spectroscopy (EIS), potentiodynamic polarization, X-ray photoelectron spectroscopy (XPS) and salt spray test. The corrosion resistance of PAGO coatings with different contents were analyzed and compared with pure PAGO-0 and the GO coatings. The anticorrosive mechanism and optimum dosage of PAGO in PVC/EP powder coating had been elaborately discussed in this paper.

Experimental

Raw materials

Polyvinyl chloride (SG-8) produced by Xinjiang Tianye Group Co., Ltd. had a relative density of 1.35–1.46, refractive index of 1.544 (20 °C). GO was purchased from Suzhou carbon feng Graphene Technology Co., Ltd. Aniline was purchased from MACKIN Co., Ltd. Ammonium persulfate (APS) was purchased from Tianjin Bodi Chemical Co., Ltd. Other synthetic chemicals, including H_2SO_4 (98%), H_2O_2 (30%), KMnO_4 and HCl , were purchased from Sinopharmaceutical Group Chemical Reagent Co., Ltd. All chemicals were analytical grade and could be used without any purification. The coated steel was purchased from Tianjin Shengrun Jie Metal material sales Co., Ltd. The steel was treated with 600, 800 and 1200 grade sandpaper and finally degreased with acetone.

Synthesis of PAGO

For the synthesis of composites, PAGO nanocomposites were prepared by in situ polymerization. 10 mg of GO tablets were added to 20 ml hydrochloric acid ($1 \text{ mol}\cdot\text{L}^{-1}$) solution by ultrasonic for 30 min, and a uniformly dispersed solution was obtained. About 1 g aniline monomer was dissolved in 20 ml deionized water, then fully mixed with GO

solution. Pour the two solutions into the 250 ml flask and stir the 30 min continuously at 10 °C. During the stirring process, ammonium persulfate (APS) dissolved in 5 ml hydrochloric acid ($1 \text{ mol}\cdot\text{L}^{-1}$) was added, and the molar ratio of aniline to ammonium persulfate was 1:1. Stir continuously for 24 h and wash the solution with deionized water and ethanol until the filtrate was colorless. After drying at 50 °C for 12 h in vacuum, PAGO complex was obtained, the average lateral size of the PAGO platelets was about 3.4 μm .

Preparation of composite coating

PAGO anticorrosive filler was added to the PVC/EP double-layer coating system. The primer used PVC resin coating modified by epoxy resin, which formed a semi-interpenetrating network structure, and the topcoat used unmodified PVC coating.

In the experiment, the preparation of the coating was divided into five steps. In the first step, the polyvinyl chloride resin, epoxy resin and various auxiliaries and fillers were added to the high-speed mixer according to the formula to complete the primary dispersion. The second step was to use the melt extrusion method to set the working temperature of the double screw extruder at 120 °C and the rotational speed of 20 rpm for melt blending. In the third step, the cryogenic liquid nitrogen crushing device was used in the experiment. After the material was melted and extruded, the material was granulated, cryogenic crushed and then sifted (180 mesh) to get the powder coating. In order to control the thickness of the coating, a certain amount of powder coating was sprayed on the tinplate of $120 \times 50 \times 0.28 \text{ mm}$ each time. In the fourth step, the electrostatic spraying method was used in the experiment. Through the role of the electrostatic generator, the spray powder coating was negatively charged, while the tinplate was positively charged, so that the powder was adsorbed on the surface of the workpiece. In the fifth step, the sprayed coating was solidified in an oven at 180 °C for 10 min, and the powder was melted and flattened to form a coating [23, 24]. The preparation process of the coating is shown in Fig. 1.

The GO coating with 0.25wt% content and the coating with PAGO content of 0, 0.25, 0.5, 1.0 and 2.0 wt% were prepared, and the filler is added to the primer and topcoat at the same time. Their abbreviations and expressions are shown in Table 1.

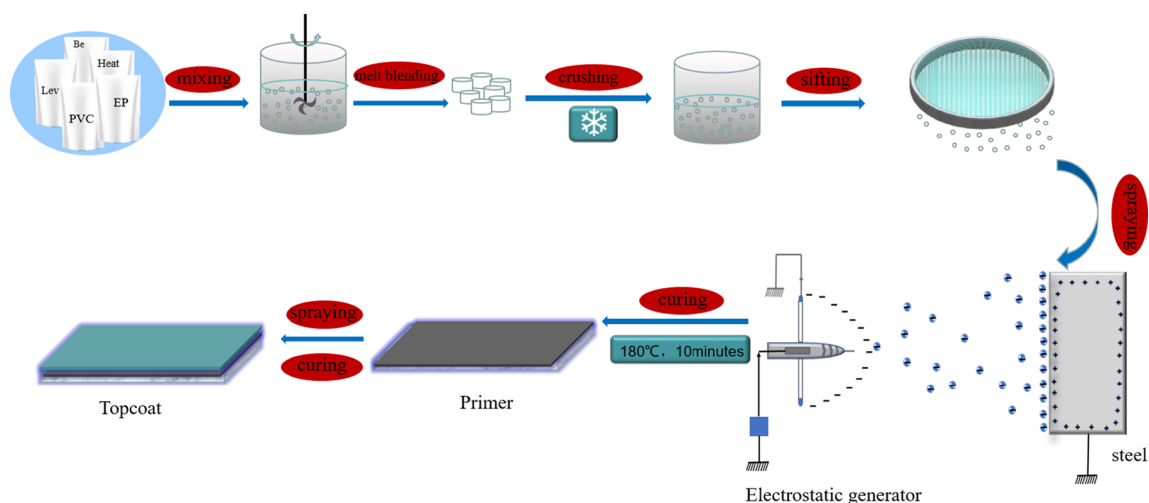


Figure 1 The preparation process of the composite coating.

Structure and morphology

Fourier transform Infrared (FT-IR) spectroscopy (Thermo-Nicolet, USA) was employed to investigate the chemical structure of GO and PAGO nanosheets. The test was performed on KBr pellet within wavenumber range of 400-4000 cm^{-1} . The phase composition of GO and PAGO nanosheets was examined by XRD analysis (Bruker D8 Advance) with Cu-ka filament and X-ray wavelength of 1.5406 Å. Scan range from 5° to 90°. The morphology of the GO, PANI and PAGO platelets as well as the cryo-fractured surface of the PVC/EP composite films were all observed by a scanning electron microscope (SEM, SU 8010, Hitachi, Japan). And corrosion products were recorded by the XPS (Thermo K alpha). The process of removing the coating to obtain the catalytic passive film was to use the knife to make X scratches on the coating and then slowly scratched the coating around the scratches along the scratches.

Mechanical properties test

The hardness of the film was tested by pencil scratch hardness method with reference to the standard ISO 15184-1998. The gloss of the film was tested by a 60° glossmeter, and the average values of the films in three different positions were calculated. The adhesion test of the film referred to ISO 2409-1992, and the adhesion strength between the coating and the substrate was tested by the marking method. The test of the impact force of the coating referred to ISO 6272-2-2002, it was stipulated that the heavy hammer of a certain quality hit the film to be tested in the form of free fall and recorded the maximum height at which the coating was not damaged (cm).

Salt spray test

The coated steel specimens were under salt spray testing in a Q-FOG Cyclic Corrosion Tester. The coated specimens were under X-cut and exposed to 3.5wt% NaCl fog (pH of 6.5-7.2) for 360 h. The testing was performed at a constant temperature of 35 °C.

Table 1 Identification of the coatings with name codes and their relationship to the addition of GO and PAGO fillers

Sample ID	Meaning
GO	The coating with 0.25wt% unmodified GO was added
PAGO-0	The coating without PAGO and GO
PAGO-0.25	The coating with 0.25wt% PAGO was added
PAGO-0.5	The coating with 0.5wt% PAGO was added
PAGO-1.0	The coating with 1.0wt% PAGO was added
PAGO-2.0	The coating with 2.0wt% PAGO was added

After testing, the specimens were assessed according to ISO 4628–2016 standard.

Electrochemical test

The electrochemical test was carried out by Zaher electrochemical workstation, and the coating was tested by polarization curve method and electrochemical impedance spectroscopy. The coated steel sheet was fixed on the electrolytic cell, and 3.5 wt% NaCl (mass fraction) solution was used as the electrolyte solution. A three-electrode system was used in the experiment, in which the working electrode was coated/metal composite electrode, the auxiliary electrode was graphite rod electrode, the reference electrode was silver/silver chloride electrode, and the exposure area was 1cm^2 . Before the experiment, the reference electrode was compared with the standard electrode for relative potential correction. The frequency range of electrochemical impedance spectroscopy was set to $100\text{ kHz} \sim 0.01\text{ Hz}$, the test voltage was open circuit voltage, and the amplitude of sine wave excitation signal was 0.2 mV .

Contact angle test

The contact angle measuring instrument (PT-705A, China) was used to measure the wettability of the liquid on the surface of the film. In this experiment, the static contact angle of distilled water was measured under the condition of temperature $25 \pm 2\text{ }^\circ\text{C}$ and humidity $30 \pm 5\%$.

Results and discussion

Structure and morphology

FT-IR analysis

The chemical structures of GO and GO-PANI nanosheets were characterized by FT-IR. According to Fig. 2a, GO had characteristic peaks at 1730 and 1410 cm^{-1} , corresponding to the extension of C=O and C-O bonds of COOH group, respectively. The stretching of C-O bond related to the epoxide groups, the stretching of aromatic C=C, and the intensive and broad peak O-H of carboxylic groups can be seen at 1200 , 1630 and 3440 cm^{-1} , respectively. These all conformed that the epoxy, hydroxyl and carboxylic

groups were present on the GO nanosheets that were in accordance with the results reported in the literature [25–28]. According to the FT-IR spectrum of GO-PANI, the characteristic peaks of PANI and GO could be observed. The main characteristic peaks related to PANI structure appeared at 1630 , 1510 and 1330 cm^{-1} , corresponding to the C=C contraction of the benzene ring, the C=N contraction of the quinone ring and the C-N extension [29–31]. The band appearing in the range of $650 \sim 850\text{ cm}^{-1}$ wave number was related to the bending deformation outside the plane. These observations confirmed the successful polymerization of aniline on GO tablets. The polymerization mechanism of aniline on the oxide film was shown in Fig. 2c. It had been reported that aniline formed hydrogen bond forces with oxygen-containing functional groups in GO through -NH- group. The polymerization of aniline into PANI could be carried out in different steps, as shown in Fig. 2c.

XRD analysis

According to Fig. 2b, a dense characteristic diffraction peak corresponding to the layer spacing $d = 0.8999\text{ nm}$ could be seen at $2\theta = 9.82^\circ$. This interlayer distance was due to the presence of oxygen-containing groups, namely hydroxyl, carboxyl and epoxy groups on the GO sheet [32]. The existence of wide peak in PANI meant that both amorphous region and crystalline region existed at the same time. On the other hand, the XRD map of PAGO showed a sharp peak compared with PANI, which could be explained by the synthesis of highly ordered PANI chains on the surface of GO. And the characteristic peak of PAGO appeared at $2\theta = 9.18^\circ$. According to the Bragg equation, the layer spacing of GO was $d = 0.8999\text{ nm}$ and the layer spacing of PAGO was $d = 0.9626\text{ nm}$, indicating that the interlayer spacing of GO was increased when PANI was inserted into the interlayer of GO molecules.

SEM analysis

The micrographs of the samples are depicted in Fig. 3. Figure 3b showed thin exfoliated GO nanowires with distinct edges, while PANI (Fig. 3a) showed the interconnected nanoparticle spheres. Compared with the synthesized PAGO (Fig. 3c), Fig. 3d showed that the PAGO composite retained

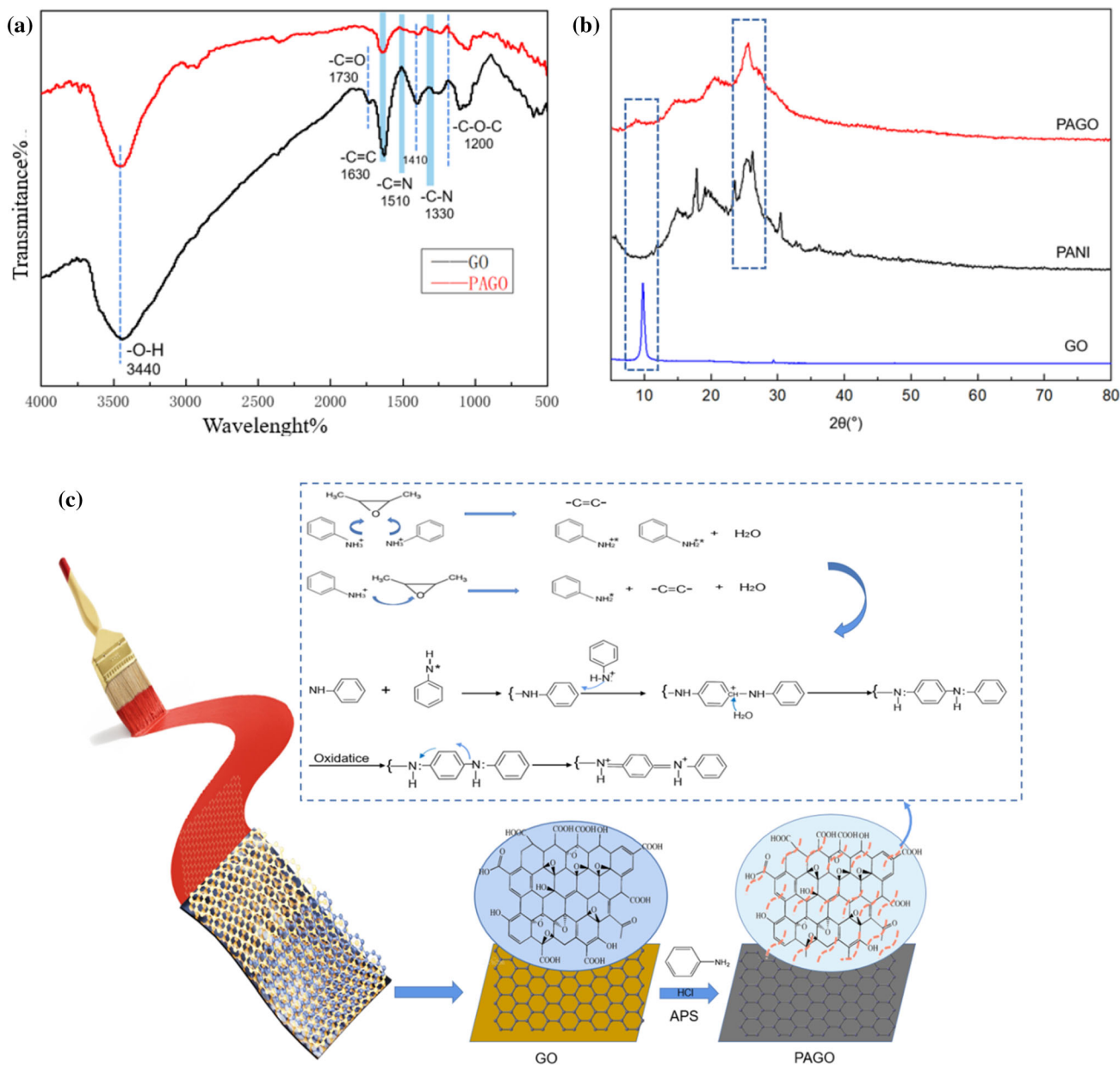


Figure 2 a FT-IR spectra for the GO and PAGO nanosheets. b X-ray diffractometer (XRD) patterns of synthesized GO, PANI and PAGO. c Schematic illustration of PAGO polymerization with the presence of APS.

the layered structure of GO, and the PANI intercalated in the lamellar GO structure was uniformly embedded in the GO layer in a chain, thus weakening the surface energy of GO and enhancing the dispersion of PANI in the coating. The cross-sectional structure of the coating was observed (Fig. 3e), and the coating showed obvious layered structure, indicating that the coating had good structural compactness. Figure 3f further confirmed the existence of the double coating.

Gloss and contact angle analysis

Figure 4 showed the gloss and contact angle measurements for the six samples. The GO coating had a contact angle of 90.84°. This was because there were a large number of hydrophilic oxygen-containing active groups on the surface of GO, which made GO have strong surface activity and wettability [33, 34]. The contact angle of the PAGO-0 coating was about 86.87°, which may be due to the large number of pores on the coating surface and the easy adhesion

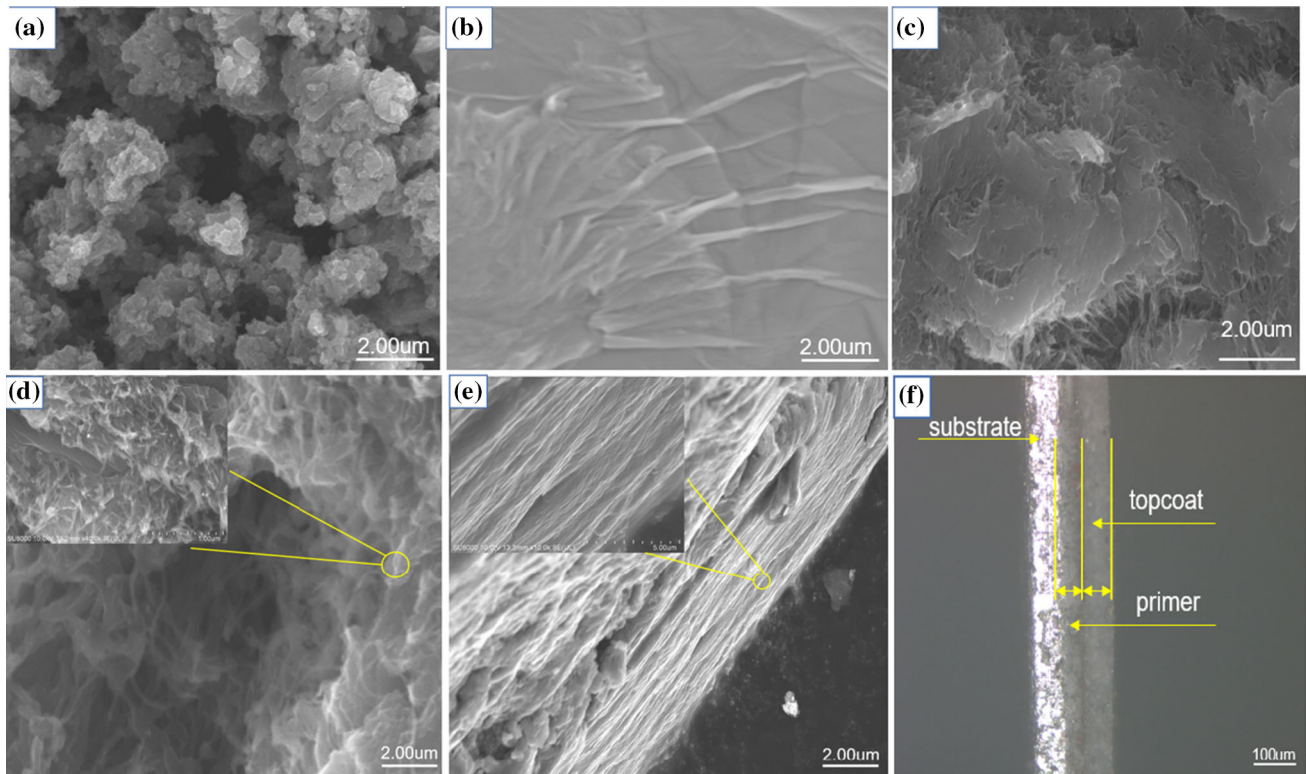


Figure 3 Scanning electron microscopy (SEM) images of the coatings with PANI **a**, GO **b**, PAGO **c**, the PAGO **d**, the cross section of the coating **e**, and the double structure of the coating under microscope **f**.

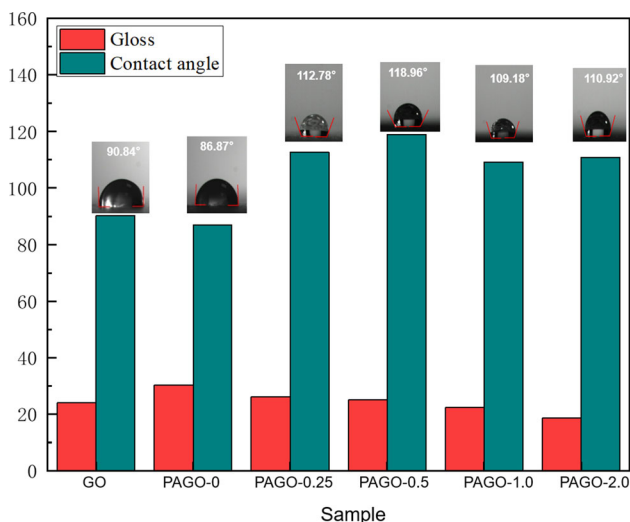


Figure 4 Gloss and contact angle of the film with different amount and kinds of corrosion fillers.

and penetration of the corrosive medium. When PAGO filler was added to PVC/EP substrate, the contact angle of the coating was greater than 90° , indicating that the coating was a hydrophobic coating, which inhibited the adhesion of the corrosive

medium. Nevertheless, due to the good mechanical properties of GO during curing, the part of the PAGO on the surface layer could not be melted, and the leveling process was limited and the gloss was low. For 0.5wt% PAGO samples, the contact angle increased to 118.96° . When the content of PAGO increased further, the contact angle decreased, mainly because the excessive PAGO increased the probability of agglomeration, and the excess filler cannot wrap and float on the surface of the coating, resulting in uneven surface of the coating.

SEM analysis of cross section of coating

To further explore the dispersion of PAGO in the coating, six samples were observed under scanning electron microscope (Fig. 5). It can be seen that for the GO coating (Fig. 5a), there was obvious agglomeration in the coating because of the large surface energy of GO. For the PAGO-0 (Fig. 5b), there were more pores in the coating, showing an uneven distribution. For the coatings with different PAGO content, it can be seen that when the content of PAGO was 0.25wt% and 0.5wt%, the dispersion of PAGO had the best

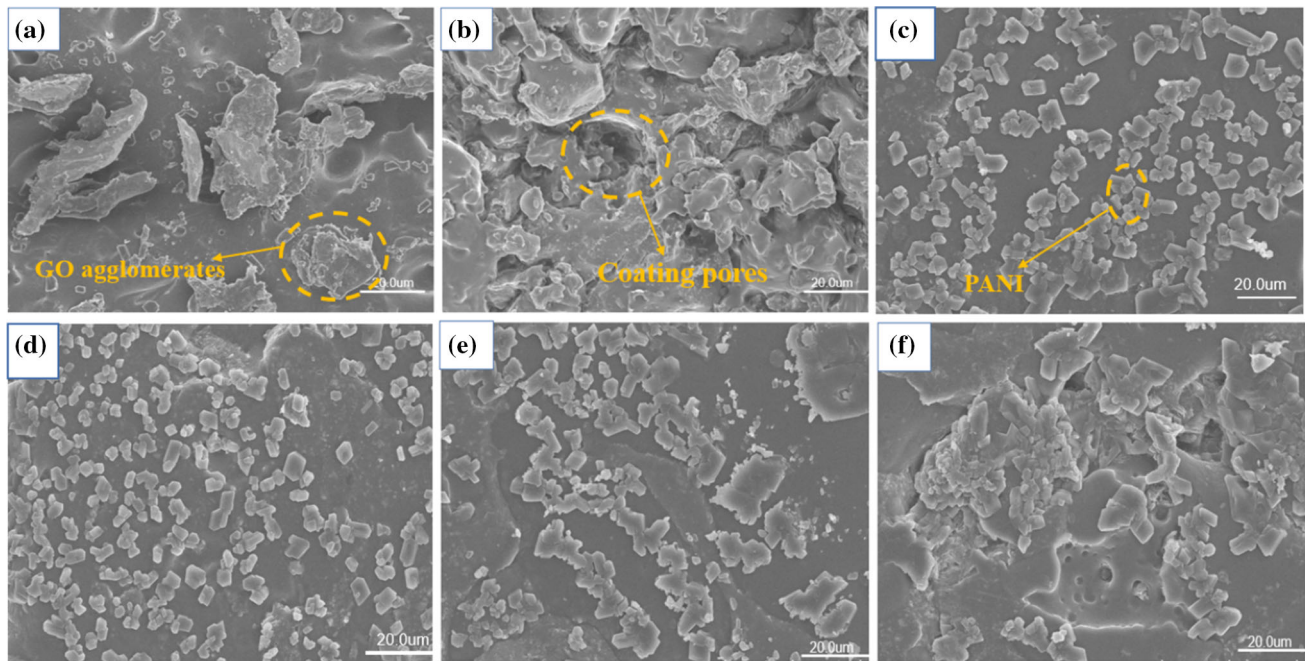


Figure 5 SEM images of the fracture surface of the sample **a** GO; **b** PAGO-0; **c** PAGO-0.25; **d** PAGO-0.5; **e** PAGO-1.0; **f** PAGO-2.0.

dispersion. With the increase of PAGO content, a large number of agglomerations began to appear in the coating, resulting in the formation of more defects. It showed that the intercalation of PANI into GO can effectively improve the dispersion of the two in the coating, but excessive PAGO content would increase the probability of agglomeration.

Salt spray analysis

The anticorrosive performance was also determined by salt spray test, which was carried out in salt-fog test box. Figure 6 showed the state of six-coating substrates after accelerated corrosion tests at different times. Blistering and corrosion products appeared around the scratches after 6 h exposure of the steel sample with non-corrosive packing. The coating around the scratches produced more and more blisters as the exposure time increased. The main reason was that the corrosion medium diffused from the scratch and penetrated into the coating through the micropores in the coating structure. Compared with the coating with PAGO filler, the number of corrosion products and blisters formed near the scratch was significantly less than that of GO coating and PAGO-0 coating after 15 days exposure. The fundamental reason for this was that the small molecular PAGO fillers filled up for the pores in the coating and

prolonged the invasion path of the corrosion medium. At the same time, at the initial stage of corrosion, well-dispersed PAGO could timely transfer the electrons lost in the anodic reaction to the coating surface in time [35–37], which can effectively delay the further occurrence of the corrosion reaction.

Mechanical property analysis

Table 2 showed the mechanical properties of different samples, such as adhesion, pencil hardness, impact force and apparent morphology. It can be seen that the hardness and impact resistance of the PVC/EP coating can be improved by adding PAGO. When the mass fraction of PAGO was 0.25wt% and 0.5wt%, respectively, the hardness of the composite coating could reach $> 6H + 1750$ g, with the best impact resistance and adhesion. However, due to the excellent mechanical properties of PAGO, PAGO had good compatibility with PVC/EP when blended with PVC/EP, which compensated the structural defects of the coating, improved the rigidity and bonding strength of PVC/EP and increased the hardness of the coating. However, when the mass fraction of PAGO continued to increase, the viscosity of the coating increased greatly, while the dispersion of PAGO became worse because of agglomeration,

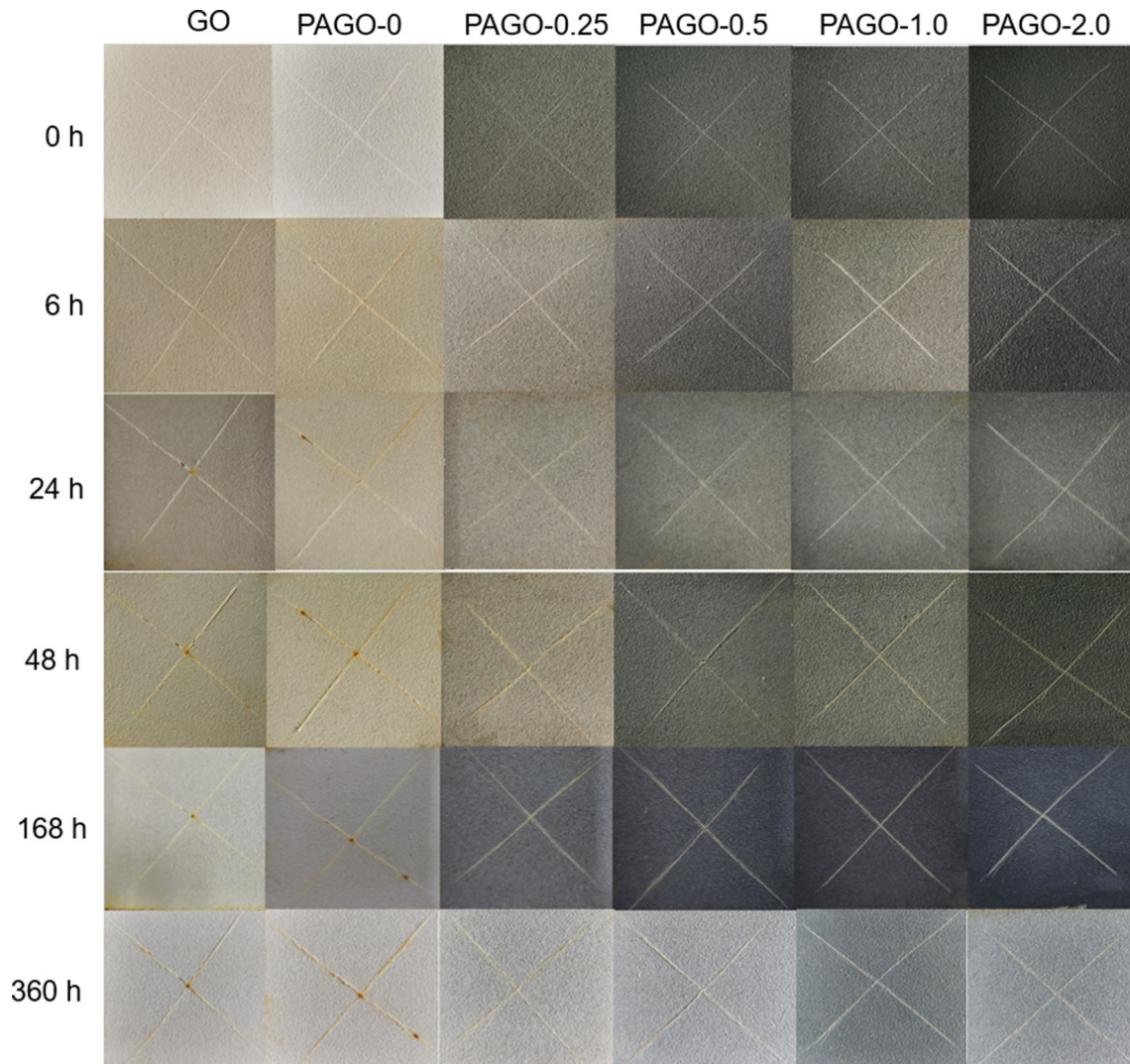


Figure 6 Photographs of coatings with different amounts of PAGO and GO test panels immersed in salt spray chamber for different exposure time.

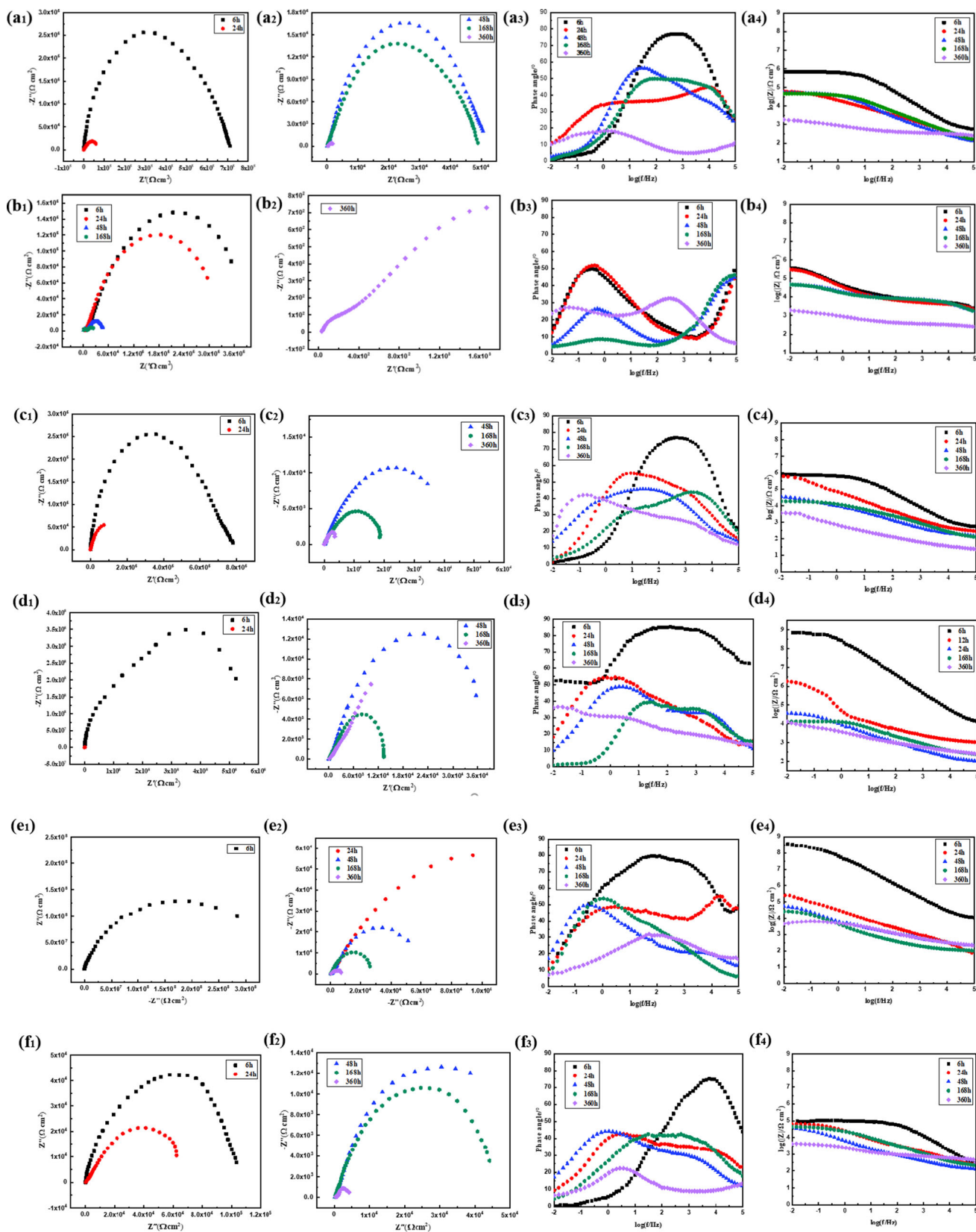
Table 2 Effect of the amount and kinds of corrosion fillers on the mechanical properties of the film

Sample	Adhesion/level	Pencil hardness	Impact strength/cm	Appearance of the film
GO	2	6H + 1750 g	Frontal and opposite impact 45	Flat
PAGO-0	2	6H + 750 g	Frontal and opposite impact 40	Smooth
PAGO-0.25	1	> 6H + 1750 g	Frontal impact 50, opposite impact 45	Flat
PAGO-0.50	1	> 6H + 1750 g	Frontal and opposite impact 50	Flat
PAGO-1.00	2	6H + 1750 g	Frontal and opposite impact 50	Not smooth and uneven
PAGO-2.00	2	6H + 1750 g	Frontal impact 50, opposite impact 45	Not smooth and uneven

which led to the decrease of the mechanical properties of the coating.

EIS analysis

Figure 7 showed the Bode plot and Nyquist plot obtained by electrochemical impedance spectroscopy



◀ **Figure 7** Bode plot and Nyquist plot of coatings with GO and different PAGO content obtained during immersion in 3.5wt% NaCl solution up to 360 h. (a₁, a₂, a₃)GO; (b₁, b₂, b₃)PAGO-0; (c₁, c₂, c₃)PAGO-0.25; (d₁, d₂, d₃)PAGO-0.5; (e₁, e₂, e₃)PAGO-1.0; (f₁, f₂, f₃)PAGO-2.0;

of the coatings with GO and different PAGO contents. All the coatings were immersed in 3.5wt% NaCl solution to monitor the corrosion resistance trend of the coating from 6 to 360 h. The Nyquist diagram showed that the sample had both capacitive behavior and diffusion behavior. At the initial stage of immersion, it showed a large diameter capacitive arc, indicating a good barrier performance. The value of $\log |Z|$ corresponding to the platform of the solution resistance appeared in the high frequency region, the platform corresponding to the coating resistance appeared in the low frequency region, and the phase angle reached the maximum in a wide range. With the extension of immersion time, the amount of electrolyte penetration into the coating increased, the coating capacitance increased gradually, and the coating resistance decreased with the extension of immersion time. In the Bode diagram, the $\log |Z|$ curve moved toward low frequency, and the phase angle decreased gradually. When the electrolyte reached saturation after penetrating into the coating for a period of time, it could be seen that the diagonal of the coating capacitance corresponding to the high frequency in the Bode diagram no longer moved toward the low frequency over time but overlapped each other [38, 39]. However, when the electrolyte solution permeated to the coating/substrate interface, corrosion microbatteries would be formed at the interface.

It can be seen from Fig. 7 (a₁ ~ a₃) that for GO coating, the diameter of capacitive arc decreased with time, after soaking for 360 h, the impedance modulus $|Z|_{0.01 \text{ Hz}}$ decreased to $10^3 \Omega \text{ cm}^2$, and the high frequency phase angle decreased to 10° . This was because unmodified GO was easy to reunite in the coating, resulting in the formation of more defects. For the PAGO-0wt% coating in Fig. 7 (b₁ ~ b₃), after soaking for 360 h, the coating showed obvious diffusion, the impedance modulus decreased to $10^3 \Omega \text{ cm}^2$ and the high frequency phase angle decreased to 5° . This was because the resin matrix of the coating generally had pores, resulting in a large number of corrosion media entering to erode the metal. It can be

seen from Fig. 7 (c₁ ~ c₃) that for PAGO-0.25wt% coating, with the increase of immersion time, the impedance modulus $|Z|_{0.01 \text{ Hz}}$ decreased from $10^6 \Omega \text{ cm}^2$ to $10^3 \Omega \text{ cm}^2$. After soaking for 360 h, the high frequency phase angle decreased to 10° . The fundamental reason for this was that with the increase of soaking time, the invasion of corrosive media increased and the blocking effect was weakened. At the same time, more and more electrons were lost on the surface of the substrate, and PAGO was not enough to transmit a large number of electrons timely, resulting in stacking, affecting the formation of the passivation layer and reducing the protective function of the substrate. As can be seen from Fig. 7 (d₁ ~ d₃), for PAGO-0.50wt% coating, at the initial stage of immersion, the phase angle observed in the high frequency range was close to 90° , and the impedance modulus $|Z|_{0.01 \text{ Hz}}$ was as high as $10^9 \Omega \text{ cm}^2$, and the diagonal lines corresponding to the coating capacitance at the high frequency end overlapped each other in the middle stage of immersion. After soaking for 360 h, the coating of PAGO-0.5 had the maximum impedance value in all samples. This was because an appropriate amount of PAGO can not only give full play to its lamellar shielding, but also transmit the electrons lost on the substrate surface timely, and induce a passivation layer at the interface damage to further protect the substrate, so that the interface corrosion was in a very slow process. As can be seen from Fig. 7 (e₁ ~ e₃), for PAGO-1.00wt% coating, the phase angle of high frequency (10^5 Hz) was close to 85° after soaking for 6 h, the values of $|Z|_{0.01 \text{ Hz}}$ were close to $10^9 \Omega \text{ cm}^2$. After soaking for 360 h, the high frequency phase angle decreased to 20° . Compared with PAGO-0.50wt% coating, the corrosion resistance of PAGO-1.00wt% coating decreased slightly, because the excess of PAGO which was not wrapped by resin began to agglomerate, resulting in the increase of porosity of the coating, which will make the invasion of the corrosion medium relatively fast. As can be seen from Fig. 7 (f₁ ~ f₃), for PAGO-2.00wt% coating, the phase angle of high frequency (10^5 Hz) was close to 80° after soaking for 6 h, the values of $|Z|_{0.01 \text{ Hz}}$ was close to $10^5 \Omega \text{ cm}^2$. After soaking for 360 h, the high frequency phase angle decreased to 15° . This was due to the fact that with the increase of PAGO, excess GO tended to agglomerate, resulting in more defects, and the effect of galvanic corrosion on the damaged

coating was greater than the catalytic passivation of PANI, which caused damage to the substrate.

Therefore, it can be seen that due to the blocking effect of PAGO, the invasion path of the corrosion medium was increased, the infiltration rate of the corrosion medium was delayed, and the electrons lost in the anodic reaction could be transferred to the coating surface in time because of the conductivity of PANI, which could effectively delay the further occurrence of the corrosion reaction and make the interface corrosion in a very slow process [40–43]. When the content of PAGO was 0.50wt%, the dispersion in the coating was the best, which can not only give full play to the shielding of PAGO sheet, but also effectively build the formation of conductive network and transfer the electrons lost by the substrate in time. Moreover, PANI with redox ability could effectively exert its catalytic redox ability under the premise of uniform dispersion, which could induce the formation of catalytic passive film on the surface of the substrate and achieve long-term and effective protection against the substrate.

In order to accurately explain the protective performance of the coating, a suitable equivalent circuit was used to fit the EIS data under different immersion time. Figure 8 showed the equivalent circuit diagram for different periods, where R_s was the solution resistance, R_c was the coating resistance, C_c was the coating capacitor, R_{ct} was the charge transfer resistor, C_{dl} was the double layer capacitor. The electrical equivalent circuit model A in Fig. 8 was used for the fitting the EIS data of Fig. 7(d₁) and Fig. 7(e₁), and the rest belong to model B.

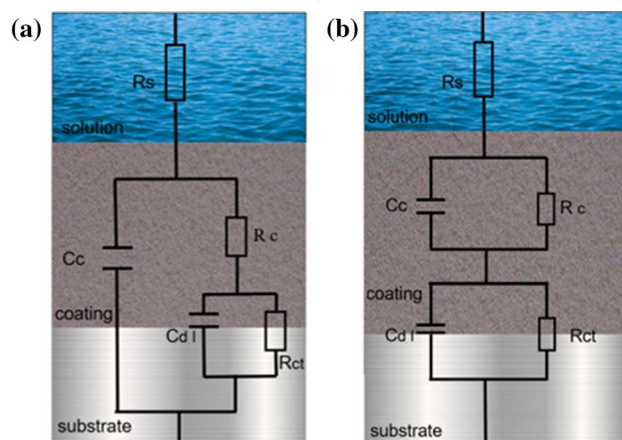


Figure 8 Equivalent circuit used to fit the EIS data.

First of all, the EIS diagram in the middle stage of immersion showed the characteristics of two time constants, the time constant corresponding to the high frequency end came from the contribution of the coating capacitance and the coating resistance, and the time constant corresponding to the low frequency end came from the contribution of the double layer capacitance of the interface blistering part and the transfer resistance of the metal corrosion reaction. The electrolyte solution infiltrated into the coating through the micropores on the surface of the coating and reached the interface of the coating substrate. The blistering in the interface area was also local and corresponded to the micropore resistance. Therefore, it was reasonable to use the model in Fig. 8 as the equivalent circuit of EIS in the middle of immersion. Secondly, due to the barrier effect of a large number of additives, it was very difficult for the electrolyte solution to penetrate into the organic coating. The electrolyte solution sinuously infiltrated inward along the gap between the particles, and the direction of ion mass transfer was not parallel to the direction of concentration gradient. The charge–discharge process of the coating and the corrosion reaction of the substrate metal were little affected by the mass transfer process, so the EIS of this period was described by the equivalent circuit of Fig. 8a. It corresponded to Fig. 7(d₁) and Fig. 7(e₁), the impedance values were all above 10^6 , and the rest belong to Fig. 8b. This was because with the increase of the filling amount of corrosion medium, the interface micropores also increased, resulting in an increase in the number of corrosion microbattery. At the same time, the electrolyte behind would slowly and uniformly infiltrate into the coating, resulting in a uniform distribution of corrosion microbattery at the interface, so the equivalent circuit of Fig. 8b was used to describe it.

The effective circuit element information such as transmission resistance (R_{ct}), coating capacitor (C_c) and coating resistance (R_c) could be obtained by ZVIEW fitting. As shown in Fig. 9, the EIS data were fitted by an equivalent circuit containing different elements including total resistance R_t ($R_t = \text{film resistance } (R_c) + \text{charge transfer resistance } (R_{ct})$) [23, 44]. The data extracted are reported in Table 3. Also, the impedance ($|Z|_{0.01 \text{ Hz}}$) values were provided for these samples in Table 3. On the whole, The capacitance of the coating increased with the immersion time, and the total resistance R_t of the

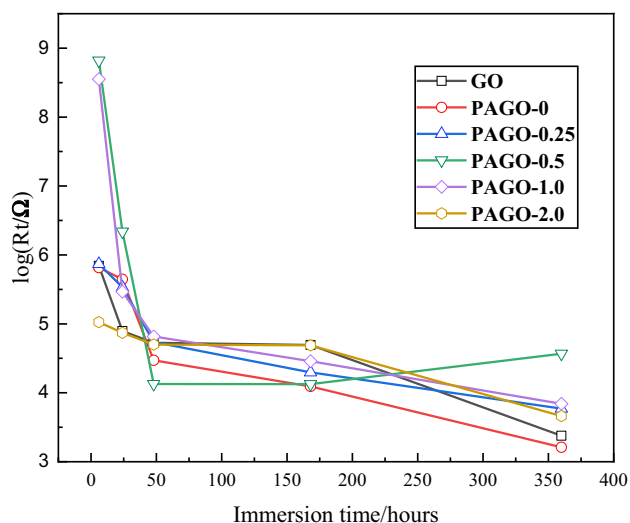


Figure 9 Total coating resistance obtained from equivalent circuit model for coatings with GO and different PAGO content exposed to 3.5wt% NaCl solution for up to 360 h.

coating decreased, indicating that the protection performance decreased with the increase of the intrusion of corrosive media [45, 46]. Compared with GO, PAGO-0 and PAGO coating, it was obvious that PAGO coating had the best corrosion resistance, with the highest R_t and $|Z|$ value. In addition, With the increase of PAGO content, the values of R_c first increased and then decreased. Therefore, it showed that the shielding effect of less PAGO on the corrosion medium was weak, and more PAGO tended to form agglomeration in the coating, leading to further corrosion of the substrate. Under the same conditions, the R_t and $|Z|$ values of PAGO-0.5 samples were the highest. This was mainly due to the good dispersion of 0.5wt% PAGO, which improved the densification of the coating and further prevented the corrosion reaction [47, 48].

Tafel analysis

The corrosion inhibition mechanism of PAGO coating on substrate was investigated by potentiodynamic polarization test. Figure 10 showed the polarization curves of six coated steel plates (1cm^2) immersed in 3.5wt% NaCl solution for 15 days. The electrochemical parameters such as corrosion potential (E_{Corr}), corrosion current density (I_{Corr}), anode (β_a), cathode (β_b) Tafel slope and corrosion rate (C_R) obtained by polarization diagram are shown in Table 3.

Among them, the polarization resistance (R_p) can be calculated by applying the following Stern–Geary equation [49–51]:

$$R_p = \frac{\beta_a \beta_b}{2.303(\beta_a - \beta_b) I_{\text{Corr}}} \quad (1)$$

β_a and β_b are anodic slope and cathodic slope, respectively.

The corrosion rate (C_R) is calculated according to the following formula:

$$C_R = \frac{k M_m I_{\text{Corr}}}{\rho_m} \quad (2)$$

where k is a constant of 3268.6 mol/A , M_m is the molar molecular weight (56 g/mol) of the metal substrate, and ρ_m is the density (7.86 g/cm^3) of the metal substrate.

As can be seen from Table 4, compared with the blank sample (PAGO-0) and PAGO-0.5wt% coating, the corrosion potential increased by 21.34% (from -0.5886 mV to -0.7142 mV), the corrosion current decreased from $3.18 \times 10^{-5} \text{ A}$ to $1.72 \times 10^{-7} \text{ A}$, simultaneously, the corrosion rate decreased by more than 100 times (from 0.7403 to 0.0040 mpy). This was due to the fact that the well-dispersed PAGO coating could prevent the diffusion of the corrosion medium by filling the pores and microdefects in the coating. Compared with the GO coating (GO-0.25wt%), the corrosion potential increased by 31.53% (from -0.5430 to -0.7142 mV), the corrosion current decreased from $1.54 \times 10^{-5} \text{ A}$ to $1.72 \times 10^{-7} \text{ A}$, and the polarization resistance increased nearly 9 times (from $3.3054 \text{ k } \Omega/\text{cm}^2$ to $28.1112 \text{ k } \Omega/\text{cm}^2$). This was because the unmodified GO tended to agglomerate in the coating. In addition, the coating without PANI did not have the function of self-repair, which led to the decrease of corrosion resistance of the coating. For different contents of PAGO coating, it could be seen that the PAGO-0.5wt% coating steel had the highest E_{Corr} value (-0.7142 mV) and the lowest corrosion current value I_{Corr} value ($1.72 \times 10^{-7} \text{ A}$), and the corrosion rate was 0.0040 mpy. Therefore, the coating of PAGO-0.5wt% had the best corrosion resistance.

SEM analysis of coating scratch

In order to further clarify the self-healing mechanism, the SEM images of scratched coatings (PAGO-0, PAGO-0.5 coatings) after soaking in 3.5 wt% NaCl solution for 7 days are shown in Fig. 11. For the

Table 3 Impedance parameters obtained from fitting of the EIS data with the equivalent circuit shown in Fig. 8 for the coatings with GO and different PANI contents

Sample	Exposure time/h	R_t ($k\Omega\text{ cm}^{-2}$)	CPE_c		CPE_{dl}		$\log(Z _{0.01\text{ Hz}}/\Omega\text{ cm}^{-2})$
			Q_{Y0} ($\mu\Omega^{-1}\text{ cm}^{-2}\text{ s}^n$)	Q_n	Q_{Y0} ($\mu\Omega^{-1}\text{ cm}^{-2}\text{ s}^n$)	Q_n	
GO	6	694.80	0.05	0.96	0.21	0.80	5.83
	24	78.67	15.73	0.51	3.21	0.69	4.78
	48	53.22	3.06	0.84	36.61	0.44	4.72
	168	49.46	4.96	0.56	2.98	0.97	4.66
	360	2.38	627.10	0.41	0.92	0.69	3.27
PAGO-0	6	653.87	7.25	0.60	0.02	0.72	5.56
	24	442.74	8.30	0.66	0.06	0.66	5.48
	48	29.64	76.68	0.47	0.07	0.68	4.67
	168	12.35	0.11	0.64	23.18	0.61	4.67
	360	1.62	122.70	0.66	1383.00	0.42	3.29
PAGO-0.25	6	740.20	0.25	0.82	0.05	0.93	5.89
	24	339.10	5.26	0.94	6.35	0.56	5.79
	48	54.47	41.90	0.49	28.31	0.79	4.60
	168	19.83	15.55	0.58	5.75	0.68	4.27
	360	5.89	780.00	0.37	1531.00	1.00	3.56
PAGO-0.50	6	659,241.43	0.00	0.89	0.00	1.00	8.86
	24	2181.94	0.59	0.74	0.85	0.90	6.25
	48	13.39	14.19	0.52	6.43	0.89	4.56
	168	13.37	14.06	0.52	6.24	0.87	4.12
	360	36.98	160.80	0.29	128.80	0.48	4.10
PAGO-1.0	6	355,524.72	0.00	0.77	0.00	0.98	8.52
	24	293.20	1.97	0.71	10.40	0.57	5.41
	48	65.65	81.81	0.36	60.12	0.79	4.73
	168	28.77	148.50	0.47	59.12	0.79	4.42
	360	6.94	172.50	0.22	34.06	0.51	3.66
PAGO-2.0	6	105.76	0.17	0.83	0.04	0.92	4.97
	24	74.19	10.93	0.64	7.59	0.54	4.80
	48	50.12	51.99	0.62	58.06	0.48	4.61
	168	48.77	10.44	0.53	4.41	0.94	4.65
	360	4.59	125.70	0.56	37.06	0.26	3.63

PAGO-0 coating, no self-healing film was observed at the scratches of the coating in Fig. 11a, and there were more signs of corrosion spread around the scratches. In contrast, the coating with PAGO filler forms a self-healing film on the scratches, which further prevents the corrosion of the metal by the corrosion medium. The SEM results of these scratched coatings further verified the anticorrosive effect of the above catalytic passivation film on the coating. (Table 5)

XPS analysis

The surface structure of carbon steel with PAGO-0.5 coating was analyzed by XPS to understand the anticorrosion mechanism. Soak the coated carbon steel for 7 days, remove the coating, expose and analyze the surface structure of the coated carbon steel after soaking for 4 days and 7 days. Figure 12 showed iron (Fe2p), oxygen (O1s) and carbon (C1s) in its XPS spectrum. As can be seen from Fig. 12a, the coated carbon steel had peaks at 711.3 and 713.1 eV, representing the Fe2p_{3/2} peaks of Fe³⁺, and there was also a peak at 710.3 eV, which was attributed to the

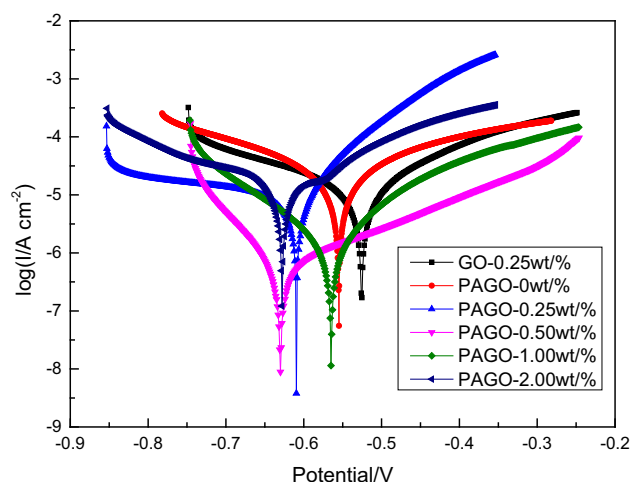


Figure 10 Polarization curves of coatings with different PAGO content and GO coatings obtained during immersion in 3.5wt% NaCl solution up to 15 d.

Fe $2p_{3/2}$ peak of Fe $^{2+}$ [37, 51–53]. At the same time, Fig. 12b showed that there were three peaks of oxygen (O1s) in iron oxides at 529.9 and 531.6 eV, corresponding to Lattice-O and Vacant-O, indicating three states of the existence of oxygen. The XPS test results showed that there was a Fe $_3$ O $_4$ and Fe $_2$ O $_3$ passivation layer between the PAGO coating and the metal substrate, which led to the positive shift of E_{corr} . At the same time, it can see from Table 5, with the extension of time, the content of FeOOH in the rust layer decreased, while the content of Fe $_3$ O $_4$ and Fe $_2$ O $_3$ increased. This is because FeOOH has a certain ionic activity and can convert to Fe $_3$ O $_4$ in the corrosive environment, which is also the process of catalytic passivation film formation[54–56]. It is further verified that the addition of PAGO filler can form a new passivation layer at the damaged coating, thus providing active protection for the substrate.

Table 4 Electrochemical corrosion measurements of coatings with different amounts of PAGO and GO samples

Specimens	E_{corr} (V)	I_{corr} (A/cm 2)	Tafel slope		R_p (k Ω /cm 2)	C_R (mpy)
			β_a (mV/dec)	β_b (mV/dec)		
GO-0.25	– 0.5430	1.54×10^{-5}	0.2107	– 0.2646	3.3054	0.3588
PAGO-0	– 0.5886	3.18×10^{-5}	0.3820	– 0.2400	2.0133	0.7403
PAGO-0.25	– 0.6376	1.12×10^{-5}	0.1122	– 0.6756	3.7237	0.2614
PAGO-0.5	– 0.7142	1.72×10^{-7}	0.1883	– 0.0118	28.1112	0.0040
PAGO-1.0	– 0.6072	3.12×10^{-6}	0.1953	– 0.1084	9.7120	0.0726
PAGO-2.0	– 0.6759	1.32×10^{-5}	0.2114	– 0.1550	2.9480	0.3068

Protection mechanism

The addition of PAGO enabled the coating to have excellent corrosion resistance, and its action mechanism is shown in Fig. 13. Firstly, it was the physical shielding of PAGO. On the one hand, its small size effect was convenient to fill in the gap of the coating, form a dense structure, hinder the invasion of the corrosion medium and delay the penetration of the corrosion medium to the metal/coating interface through the anticorrosive layer; on the other hand, its layered structure was closely arranged under the force of the interlayer effect, forming a dense physical isolation layer, prolonging the invasion path of the corrosion medium and greatly improving the shielding performance of the material. Secondly, it was the special electrical activity of PAGO. On the one hand, due to the electrical conductivity of PANI, the electrons lost on the substrate surface could be transferred to the coating surface at the initial stage of corrosion, thus effectively delaying the further occurrence of corrosion reaction. On the other hand, because PANI had redox ability, once it came into contact with the iron surface at the damaged part of the coating, it would act as a redox catalyst and catalyze the oxidation reaction on the iron surface to form a dense passivation layer composed of Fe $_2$ O $_3$ and Fe $_3$ O $_4$, which had an active protective effect on the substrate.

Conclusions

- (1) PAGO anticorrosive fillers were synthesized by in situ polymerization. FT-IR, XRD and SEM showed that PANI was successfully

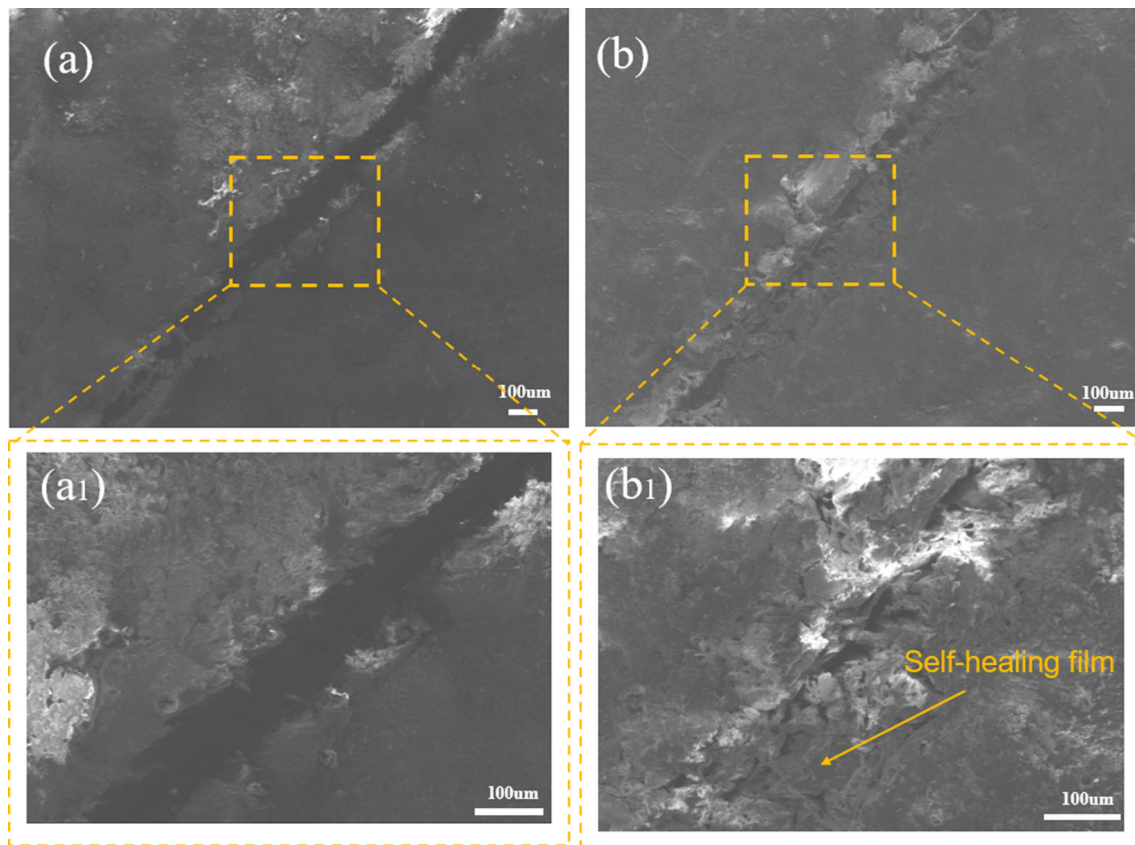


Figure 11 SEM of the scratch of the coating immersed in 3.5wt%NaCl solution for 7 days **a** PAGO-0; **b** PAGO-0.25;

Table 5 Chemical component of rust layer

Concentration(%)	Fe ₃ O ₄	Fe ₂ O ₃	FeOOH
soaked for 4 days	16.76	40.54	42.7
soaked for 7 days	18.72	52.61	28.66

intercalated into GO, to realize the uniform dispersion of PAGO in PVC/EP powder coating.

- (2) Compared with PAGO-0 and the GO coatings, the intercalation of PANI could effectively improve the dispersion of graphite oxide in PVC/EP matrix, and the coating with PAGO anticorrosive filler had excellent mechanical properties such as hardness and impact

resistance. Electrochemical analysis (EIS and Tafel) showed that the long-term anticorrosive ability of the coating could be greatly improved by adding appropriate amount of PAGO (0.5wt%).

- (3) Through the corrosion resistance test of the coating and the analysis of the corrosion products, it was concluded that the excellent corrosion resistance was attributed to two parts: (1) PAGO with good dispersion could fully show its barrier performance to prevent the penetration of corrosion medium into steel matrix. (2) PANI with complete electroactivity could transfer the electrons lost by the substrate to the surface of the coating in time and formed a passivation film composed of Fe₃O₄ and Fe₂O₃ by induction. The barrier property of GO and

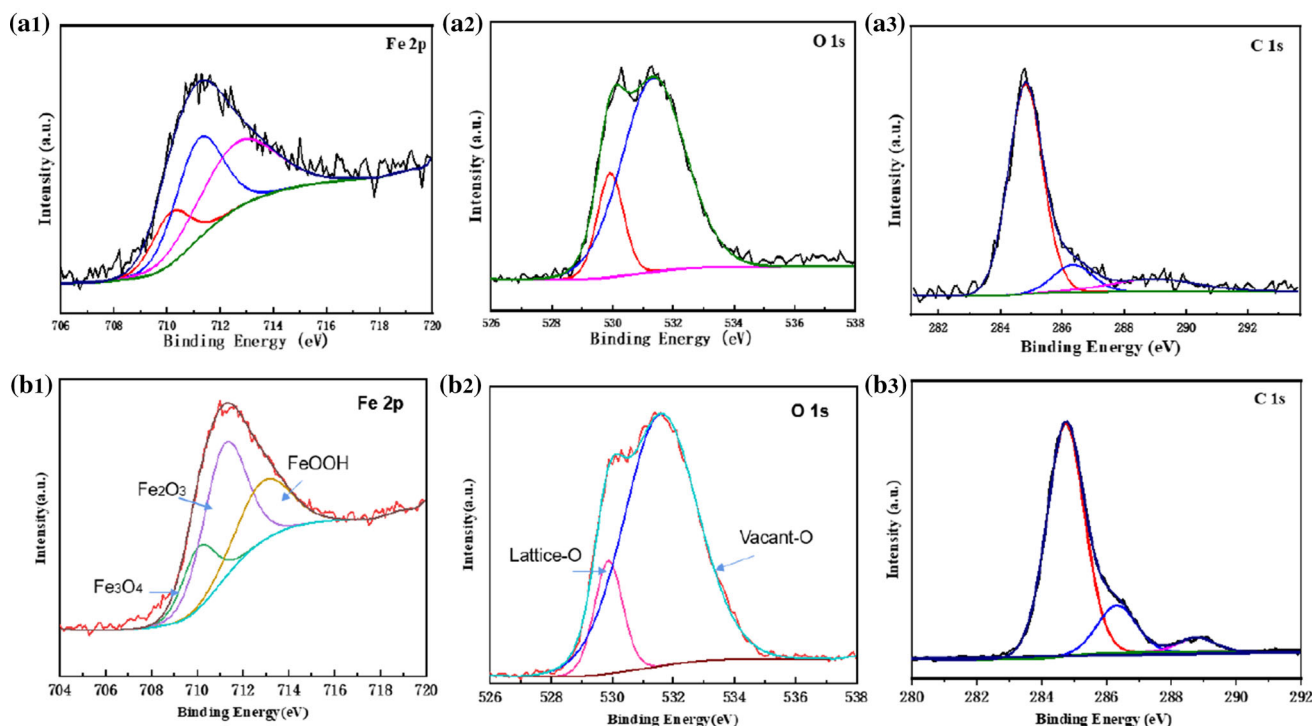


Figure 12 XPS analysis of rust layer for PAGO-0.5 coating (a₁,a₂,a₃)the coating was soaked for 4 days; (b₁,b₂,b₃)the coating was soaked for 7 days.

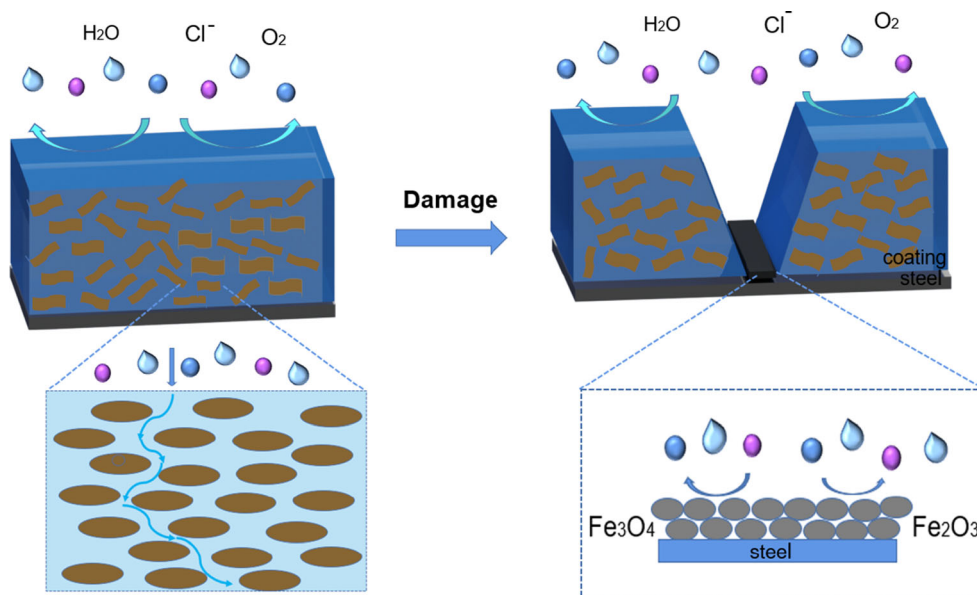


Figure 13 Schematic diagrams of coating protection mechanism.

the self-healing ability of PANI made PAGO-based PVC/EP coatings have excellent corrosion resistance.

Data availability

The data used to support the findings of this study are available from the corresponding author upon request.

Acknowledgments

This work is supported by Shandong joint fund of National Natural Science Foundation of China (U1706225), Qingdao Post Doctoral Fund (Y4KY14110N) and Open Fund of Shandong Key Laboratory of Corrosion Science (KLCS201911).

References

- [1] Yu DY, Wen SG, Yang JX et al (2017) RGO modified ZnAl-LDH as epoxy nanostructure filler: a novel synthetic approach to anticorrosive waterborne coating. *Surf Coat Technol* 326:207–215
- [2] Ding R, Chen S, Lv J (2019) Study on graphene modified organic anticorrosive coatings: A comprehensive review. *J Alloys Compd* 806:611–635
- [3] Ding R, Chen S, Lv J (2019) Research on dispersibility, orientation, functionalization and conductivity of graphene in organic anticorrosive coatings and practical problems. *Paint Coat Ind* 49:66–80
- [4] Othman NH, Ismail MC, Mustapha M et al (2019) Graphene-based polymer nanocomposites as barrier coatings for corrosion protection. *Prog Org Coat* 135:82–99
- [5] Ren Q, Chen J, Chu FQ et al (2017) Graphene/star polymer nanocoating. *Prog Org Coat* 103:15–22
- [6] Kirkland NT, Schiller T, Medhekar N et al (2012) Exploring graphene as a corrosion protection barrier. *Corros Sci* 56:1–4
- [7] Wu YQ, He Y, Chen CL et al (2020) Non-covalently functionalized boron nitride by graphene oxide for anticorrosive reinforcement of water-borne epoxy coating. *Colloids Sur A* 587:124337
- [8] Cheng LH, Liu CL, Han DJ (2019) Effect of graphene on corrosion resistance of waterborne inorganic zinc-rich coatings. *J Alloys Compd* 774:255–264
- [9] Zheng H, Guo M, Shao Y et al (2018) Graphene oxide–poly (urea–formaldehyde) composites for corrosion protection of mild steel. *Corros Sci* 139:1–12
- [10] Ma L, Wang X, Wang J et al (2021) Graphene oxide–cerium oxide hybrids for enhancement of mechanical properties and corrosion resistance of epoxy coatings. *J Mater Sci* 56:10108–10123
- [11] Liu X, Xiong J, Lv Y et al (2009) Study on corrosion electrochemical behavior of several different coating systems by EIS. *Prog Org Coat* 64:497–503
- [12] Nayak SR, Mohana KN, Hegde MB (2019) Anticorrosion performance of 4-fluoro phenol functionalized graphene oxide nanocomposite coating on mild steel. *J Fluorine Chem* 228:109392
- [13] Tian YQ, Xie YH, Dai F (2020) Ammonium-grafted graphene oxide for enhanced corrosion resistance of waterborne epoxy coatings. *Surf Coat Technol* 383:125227
- [14] Kasaeian M, Ghasemi E, Ramezanzadeh B et al (2018) Construction of a highly effective self-repair corrosion-resistant epoxy composite through impregnation of 1H-Benzimidazole corrosion inhibitor modified graphene oxide nanosheets (GO-BIM). *Corros Sci* 145:119–134
- [15] Liu CB, Zhao HC, Hou PM et al (2018) Efficient graphene/cyclodextrin-based nanocontainer: synthesis and host-guest inclusion for self-healing anticorrosion application. *ACS Appl Mater Interfaces* 10:36229–36239
- [16] Ramezanzadeh B, Bahlakeh G, Ramezanzadeh M (2018) Polyaniline–cerium oxide (PANI–CeO₂) coated graphene oxide for enhancement of epoxy coating corrosion protection performance on mild steel. *Corros Sci* 137:111–126
- [17] Sheng XX, Cai WX, Zhong L et al (2016) Synthesis of functionalized graphene/polyaniline nanocomposites with effective synergistic reinforcement on anticorrosion. *Ind Eng Chem Res* 31:8576–8585
- [18] Xiao FJ, Qian C, Guo MY (2018) Anticorrosive durability of zinc-based waterborne coatings enhanced by highly dispersed and conductive polyaniline/graphene oxide composite. *Prog Org Coat* 125:79–88
- [19] Jafarzadeh S, Claesson PM, Sundell P-E et al (2014) Nanoscale electrical and mechanical characteristics of conductive polyaniline network in polymer composite films. *ACS Appl Mater Interfaces* 6:19168–19175
- [20] Meroufel A, Deslouis C, Touzain S (2008) Electrochemical and anticorrosion performances of zinc-rich and polyaniline powder coatings. *Electrochim Acta* 53:2331–2338
- [21] Qiu CC, Liu DM, Jin K et al (2017) Electrochemical functionalization of 316 stainless steel with polyaniline–graphene oxide: corrosion resistance study. *Mater Chem Phys* 198:90–98
- [22] Mafi R, Mirabedini SM, Naderi R et al (2008) Effect of curing characterization on the corrosion performance of polyester and polyester/epoxy powder coatings. *Corros Sci* 50:3280–3286
- [23] Parhizkar N, Shahrabi T, Ramezanzadeh B (2017) A new approach for enhancement of the corrosion protection properties and interfacial adhesion bonds between the epoxy coating and steel substrate through surface treatment by covalently modified amino functionalized graphene oxide film. *Corros Sci* 123:55–75
- [24] Izadinia M, Soltani R, Sohi MH (2020) Formation of vertical cracks in air plasma sprayed YSZ coatings using unpyrolyzed powder. *Ceram Int* 46:22383–22390

- [25] Li D, Muller MB, Gilje S et al (2008) Processable aqueous dispersions of graphene nanosheets. *Nat Nanotechnol* 3:101–105
- [26] Lin YT, Don TM, Wong CJ (2019) Improvement of mechanical properties and anticorrosion performance of epoxy coatings by the introduction of polyaniline/graphene composite. *Surf Coat Technol* 374:1128–1138
- [27] Mooss VA, Bhopale AA, Deshpande PP (2017) Graphene oxide-modified polyaniline pigment for epoxy based anticorrosive coatings. *Chem Pap* 71:1515–1528
- [28] Ramezanzadeh B, Mohamadzadeh Moghadam MH, Shohani N et al (2017) Effects of highly crystalline and conductive polyaniline/graphene oxide composites on the corrosion protection performance of a zinc-rich epoxy coating. *Chem Eng J* 320:363–375
- [29] Lindfors T, Ivaska A (2005) Raman based pH measurements with polyaniline. *J Electroanal Chem* 580:320–329
- [30] Trchov M, Sedenkov I, Tobolkov E et al (2004) FTIR spectroscopic and conductivity study of the thermal degradation of polyaniline films. *Polym Degrad Stab* 86:179–185
- [31] Trchova M, Stejskal J (2011) Polyaniline: the infrared spectroscopy of conducting polymer nanotubes (IUPAC Technical Report). *Pure Appl Chem* 83:1803–1817
- [32] Pouget JP, Jdzefowicz ME, Epstein AJ et al (1991) X-ray Structure of Polyaniline. *Macromolecules* 24:779–789
- [33] Dreyer DR, Park S, Bielawski CW et al (2010) The chemistry of graphene oxide. *Chem Soc Rev* 39:228–240
- [34] Chang KC, Hsu CH, Lu HI et al (2014) Advanced anticorrosive coatings prepared from electroactive polyimide/graphene nanocomposites with synergistic effects of redox catalytic capability and gas barrier properties. *Express Polym Lett* 8:243–255
- [35] Taheri NN, Ramezanzadeh B, Mahdavian M (2018) In-situ synthesis of Zn doped polyaniline on graphene oxide for inhibition of mild steel corrosion in 3.5wt.% chloride solution. *J Ind Eng Chem* 63:322–339
- [36] Vadukumpully S, Paul J, Mahanta N et al (2011) Flexible conductive graphene/poly (vinyl chloride) composite thin films with high mechanical strength and thermal stability. *Carbon* 49:198–205
- [37] Chen C, Qiu SH, Cui MJ (2017) Achieving high performance corrosion and wear resistant epoxy coatings via incorporation of noncovalent functionalized graphene. *Carbon* 114:356–366
- [38] Liu L, Hu JM, Zhang JQ et al (2010) Evaluation of protectiveness of organic coatings by means of high-frequency EIS measurement. *Corros Sci Prot* 22:326–328
- [39] Li ZY, Gao M, Hu JM et al (2016) Electrochemical investigation of corrosion performance of electrophoretic hybrid epoxy-silane coatings on galvanized steel. *Corros. Sci. Prot. Technol.* 28:408–414
- [40] Bandeira RM, van Drunen J, Tremiliosi-Filho G et al (2017) Polyaniline/polyvinyl chloride blended coatings for the corrosion protection of carbon steel. *Prog Org Coat* 106:50–59
- [41] Shreepathi S, Bajaj P, Mallik BP (2010) Electrochemical impedance spectroscopy investigations of epoxy zinc rich coatings: role of Zn content on corrosion protection mechanism. *Electrochim Acta* 55:5129–5134
- [42] Teng S, Gao Y, Cao F et al (2018) Zinc-reduced graphene oxide for enhanced corrosion protection of zinc-rich epoxy coatings. *Prog Org Coat* 123:185–189
- [43] Gupta RK, Malviya M, Verma C et al (2017) Aminoazobenzene and diaminoazobenzene functionalized graphene oxides as novel class of corrosion inhibitors for mild steel: experimental and DFT studies. *Mater Chem Phys* 198:360–373
- [44] Yu ZX, Lv L, Ma Y et al (2016) Covalent modification of graphene oxide by metronidazole for reinforced anti-corrosion properties of epoxy coatings. *RSC Adv* 22:18217–18226
- [45] Mourya P, Banerjee S, Singh M (2014) Corrosion inhibition of mild steel in acidic solution by *Tagetes Erecta* (marigold flower) extract as a green inhibitor. *Corros Sci* 85:352–363
- [46] Tao Z, He W, Wang S et al (2012) A study of differential polarization curves and thermodynamic properties for mild steel in acidic solution with nitrophenyltriazole derivative. *Corros Sci* 60:205–213
- [47] Eddy NO, Yahaya HM, Oguzie EE (2015) Theoretical and experimental studies on the corrosion inhibition potentials of some purines for aluminum in 0.1 M HCl. *J Adv Res* 6:203–217
- [48] Mansfeld F (1976) The polarization resistance technique for measuring corrosion currents. *Adv Corrosion Sci Technol* 6:163–262
- [49] Shi H, Liu F, Han EH (2015) Surface-engineered microcapsules by layer-by-layer assembling for entrapment of corrosion inhibitor. *J Mater Sci Technol* 31:512–516
- [50] Li X, Wang F, Mao J (2019) Preparation and properties of thermosetting powder/graphene oxide coatings for anticorrosion application. *J Appl Polym Sci* 136:48264
- [51] Wei QY, Wang XT, Ning XB et al (2016) Preparation of NiSe₂/TiO₂ nanocomposite for photocathodic protection of stainless steel. *Mater Lett* 185:443–446
- [52] Ye YW, Zhang DW, Liu T et al (2019) Superior corrosion resistance and self-healable epoxy coating pigmented with silanized trianiline-intercalated graphene. *Carbon* 142:164–176

- [53] Qiu S, Liu G, Li W et al (2018) Noncovalent exfoliation of graphene and its multifunctional composite coating with enhanced anticorrosion and tribological performance. *J Alloy Comp* 747:60–70
- [54] Haile M, Sweeney CB, Lackey BA et al (2017) Ultrafast and highly localized microwave heating in carbon nanotube multilayer thin films. *Adv Mater Interfaces* 4:1700371
- [55] Qian ZJ, Li WG, Lin CS et al (2020) Rust-converting coating under heavy-duty corrosion environment and XRD mechanism analysis. *Coat and Prot* 41:1–9
- [56] Bandeira RM, Drunen JV (2018) Chemically synthesized polyaniline/polyvinyl chloride blended coatings for the corrosion protection of AA7075 aluminum alloy. *Corros Sci* 139:35–46

Publisher's Note Springer Nature remains neutral with regard to jurisdictional claims in published maps and institutional affiliations.